J. Fluid Mech. (1980), *vol.* 100, *part* 1, *pp.* 65–86
Printed in Great Britain

Unsteady natural convection in a rectangular cavity

By JOHN PATTERSON

Department of Civil Engineering,
The University of Western Australia,
Nedlands, W.A. 6009

AND JORG IMBERGER†

Department of Civil Engineering,
University of California,
Berkeley, California 94720

(Received 17 April 1978 and in revised form 14 January 1980)

The problem of transient natural convection in a cavity of aspect ratio $A \leqslant 1$ with differentially heated end walls is considered. Scale analysis is used to show that a number of initial flow types are possible, collapsing ultimately onto two basic types of steady flow, determined by the relative value of the non-dimensional parameters describing the flow. A number of numerical solutions which encompass both flow types are obtained, and their relationship to the scale analysis is discussed.

1. Introduction

The transport of heat or mass by buoyancy-induced convective motions is a mechanism which finds relevance in many physical systems; accordingly there have been numerous theoretical, experimental and numerical studies of various aspects of natural convection flows. In particular, the idealized problem of steady laminar flow in an enclosed rectangular cavity with differentially heated end walls has been extensively studied in various contexts.

These investigations have, for the most part, been concerned with cavities for which the aspect ratio A (height/length) is greater than or equal to unity. The analytical progress made by Batchelor (1954) and Gill (1966) belonged to this class, as did most of the experimental results (Eckert & Carlson 1961; Elder 1965) and the many numerical approaches (e.g. Wilkes & Churchill 1966; de Vahl Davis 1968; Newell & Schmidt 1970; Quon 1972). Although occasionally included as part of a wider study (e.g. Cotton, Ayyaswamy & Clever 1974), the small aspect-ratio case was not treated in a detailed way until Cormack, Leal & Imberger (1974), Cormack, Leal & Seinfeld (1974) and Imberger (1974) examined the problem from the analytical, numerical and experimental points of view respectively.

The three analytical papers mentioned above (Batchelor 1954; Gill 1966; Cormack, Leal & Imberger 1974) each deal with fundamentally different flow and heat transfer regimes. In the first case, Batchelor showed that, for small Rayleigh numbers based on cavity length (i.e. small horizontal temperature gradients) and large aspect ratios,

---

† Present address: Department of Civil Engineering, University of Western Australia, Nedlands, Western Australia 6009.

0022-1120/80/4518-1880 $02.00 © 1980 Cambridge University Press

the mode of heat transfer is primarily by conduction. On the other hand, the case treated by Gill (essentially fixed A and large Rayleigh number) resulted in the formation of thin boundary-layer regions driving the entire flow, with convection dominating the heat-transfer process. Finally, Cormack, Leal & Imberger determined that, for fixed Rayleigh number and sufficiently small aspect ratio, conduction was again the dominant mode of heat transfer, with the flow being driven by the temperature gradient across the cavity and the end regions merely turning the flow around.

This transition in flow regimes may be of importance in environmental flows, for which the small aspect-ratio cavity has a particular significance. A long shallow cavity with end walls at different temperatures may be regarded as an idealized model of, for example, the transfer of pollutant in estuaries or the motions set up in the epilimnion of lakes or reservoirs by non-uniform radiative heating. In many such environmental applications, the origin of the buoyancy forces is cyclic or time dependent in some sense, and, in contrast to the large aspect-ratio configuration, the forcing time scale may be small in comparison to the flow set-up time. In these cases, the transient behaviour is of interest and the question of the importance of the division of flow regimes at the transient level naturally arises.

The unsteady problem has attracted little interest and transient behaviour is rarely documented, although steady numerical solutions have been occasionally obtained by time stepping from a prescribed initial state. Apart from Wilkes & Churchill (1966), who obtained some transient results, and in different contexts (e.g. Szekely & Todd 1971) unsteady numerical or experimental results for these flows appear to be unavailable.

In this paper, a simple scale analysis is used to give some insight into the possible transient behaviour for the case $A \leqslant 1$. With the non-dimensional parameters describing the flow (the Rayleigh number Ra, the Prandtl number σ, and A) defined in the usual way, a number of possible transient flow types appear possible, depending on the value of Ra in relation to various combinations of σ and A. These regimes may be further combined to provide a broad classification of the flows into conductive, convective, or transitional, depending on the relative values of Ra, unity, and a critical Rayleigh number Ra_c, where $Ra_c = \max(\sigma^2, A^{-12})$. In the first case, $Ra < 1$, the transient flow may be described as a slow spin-up of the fluid, with conduction always dominating the heat-transfer process. The fluid velocities increase slowly to their steady values, as does the total heat transfer across the cavity. In the convective case, $Ra > Ra_c$, vertical boundary layers are formed and maintained, with convection the dominant mode of heat transfer. The approach to steady state in this case depends on the relative values of Ra and $\sigma^4 A^{-4}$; if $Ra_c < Ra < \sigma^4 A^{-4}$, the approach is again by a regular spin-up of the fluid, whereas for $Ra > \sigma^4 A^{-4}$, the velocities and total heat transfer rise sharply to peak values and approach steady state in a decaying oscillatory manner. For $1 < Ra < Ra_c$, the flow is one of transition between these extremes.

Finally, a number of numerical solutions for the special case $A = 1$ are obtained using a modified version of the finite-difference method proposed by Chorin (1968). The parameter values used in these solutions are such that the divisions in flow regimes are traversed, and the numerical results are discussed in relation to the results of the scale analysis.

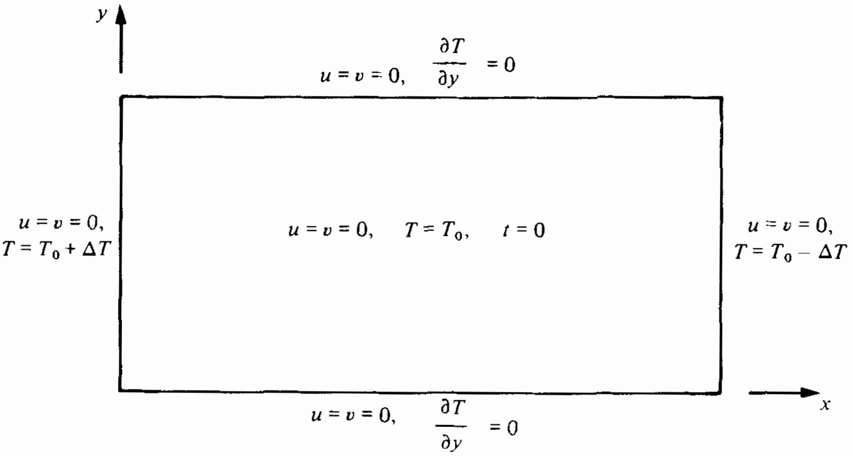

FIGURE 1. The rectangular cavity notation and boundary conditions.

2. Formulation and scale analysis

Under consideration is a closed rectangular two-dimensional cavity of length l and height h with rigid non-slip boundaries containing a Newtonian fluid initially at rest and at temperature T_0 (see figure 1). The upper and lower boundaries are insulated. At time $t = 0$, the left- and right-hand end walls are instantaneously heated and cooled respectively to temperatures $T_0 + \Delta T$ and $T_0 - \Delta T$ and thereafter maintained at these temperatures. The subsequent motion is described by the usual equations, which incorporate the Boussinesq assumption:

$$\frac{\partial u}{\partial t}+u\frac{\partial u}{\partial x}+v\frac{\partial u}{\partial y} = -\frac{1}{\rho_0}\frac{\partial p}{\partial x}+\nu\nabla^2 u, \tag{1}$$

$$\frac{\partial v}{\partial t}+u\frac{\partial v}{\partial x}+v\frac{\partial v}{\partial y} = -\frac{1}{\rho_0}\frac{\partial p}{\partial y}+\nu\nabla^2 v+g\alpha(T-T_0), \tag{2}$$

$$\frac{\partial u}{\partial x}+\frac{\partial v}{\partial y} = 0, \tag{3}$$

$$\frac{\partial T}{\partial t}+u\frac{\partial T}{\partial x}+v\frac{\partial T}{\partial y} = \kappa\nabla^2 T, \tag{4}$$

where u and v are the horizontal and vertical components of velocity, T the temperature, and p the pressure (including the hydrostatic pressure) at any point in the fluid, g the acceleration due to gravity and ν, ρ_0, α and κ the kinematic viscosity, density, coefficient of thermal expansion and conductivity of the fluid at temperature T_0. The appropriate initial and boundary conditions are

$$u = v = 0, \quad T = T_0, \quad \text{at all } x, y \text{ and } t < 0; \tag{5}$$

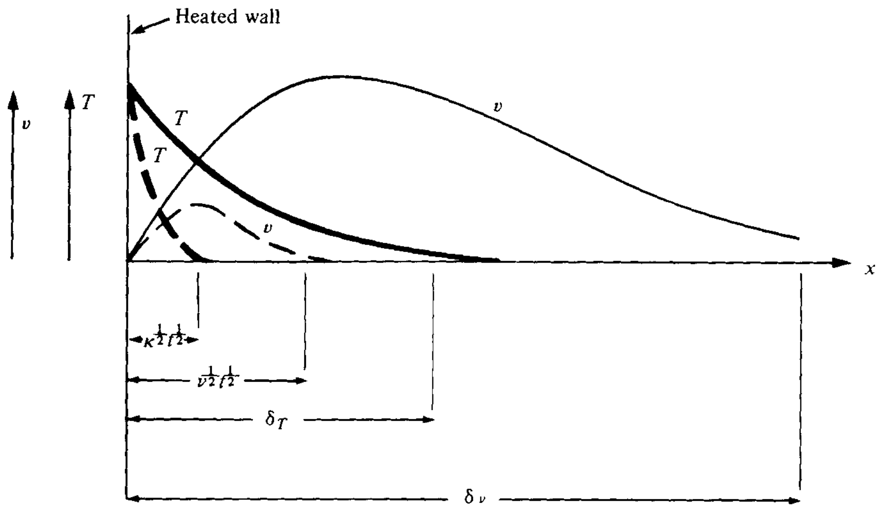

FIGURE 2. An illustration of the growth (– – – –) of the double layer on the vertical wall to the steady state (——) double-layer system at $t \sim \tau$ (equation (9)).

and

$$\begin{aligned} u = v = 0 \quad &\text{on} \quad x = 0, l, \quad y = 0, h; \\ \frac{\partial T}{\partial y} = 0 \quad &\text{on} \quad y = 0, h; \\ T = T_0 \pm \Delta T \quad &\text{on} \quad x = 0, l, \quad t \geqslant 0. \end{aligned} \tag{6}$$

A scale analysis is now applied to the set (1)–(6) to determine, firstly, the appropriate time and length scales for the initial flow near the end walls, secondly, the scales relevant to the discharge of the heated and cooled fluid into the core region of the cavity and, thirdly, the subsequent development of the flow in the core to steady state.

(a) *End-wall vertical boundary-layer growth*

As either end wall has a similar influence on the interior fluid it suffices to consider only the heated boundary region. In this region the length scale is assumed to be δ, the height scale h, the vertical velocity scale v, and the time scale τ. Implicit in the following analysis is the assumption that $\delta \ll h$; once the relevant scales have been established, the constraints imposed by this assumption will be determined.

Initially, heat is conducted into the fluid from the wall, resulting in a vertical layer of heated fluid of thickness $O(\delta_T)$, where, from (4),

$$\delta_T \sim \kappa^{\frac{1}{2}} t^{\frac{1}{2}}. \tag{7}$$

The buoyancy forces act to accelerate the fluid only over the thickness δ_T; in this layer, the unsteady inertial term of (2) is $O(v/t)$ and the viscous term $O(\nu v/\delta_T^2)$. The ratio of the unsteady inertia forces to be viscous forces in the layer is therefore $O(\sigma^{-1})$ and the correct balance for $\sigma > 1$ is between the buoyancy and viscous forces, yielding a vertical velocity scale

$$v \sim \frac{g\alpha\Delta T}{\sigma} t. \tag{8}$$

Momentum is both advected away by this velocity and diffused into the core beyond the thickness δ_T; the advection term of (2) is $O(v^2/h)$ and the ratio of the advection to the diffusion of momentum over δ_T is $O(g\alpha\Delta T t^2/\sigma^2 h)$. For $t < \sigma h^{\frac{1}{2}}/(g\alpha\Delta T)^{\frac{1}{2}}$, vorticity is therefore diffused into the core, generating a secondary viscous layer of thickness $O(\nu^{\frac{1}{2}}t^{\frac{1}{2}})$. A double-layer structure appears, as illustrated in figure 2, with the inner thermal layer governed by a buoyancy–viscous balance, and the outer viscous layer by an inertia–viscous balance.

Heat is also being convected vertically in the inner layer by the velocity (8) and the layer will continue to grow until the heat conducted in from the boundary balances that convected away. The convection term of (4) is $O(v\Delta T/h)$ and the conduction term $O(\kappa\Delta T/\delta_T^2)$; using (7) and (8) this balance yields a growth time scale for the thermal boundary layer,

$$t = \tau \sim \frac{h^2}{\kappa Ra^{\frac{1}{2}}}, \tag{9}$$

at which time the velocity and length scales have become

$$v \sim \frac{\kappa Ra^{\frac{1}{2}}}{h} \tag{10}$$

and

$$\delta_T \sim \frac{h}{Ra^{\frac{1}{4}}}, \tag{11}$$

where the Rayleigh number Ra is defined in the usual way:

$$Ra = \frac{g\alpha\,\Delta T\, h^3}{\nu\kappa}.$$

The scales (10) and (11) are identical, with appropriate change in notation, with those obtained by Braun, Ostrach & Heighway (1961), and Gill (1966) for the corresponding steady-state problem.

Thus the inner thermal layer grows until it has reached a thickness δ_T in time τ; since $\tau < \sigma h^{\frac{1}{2}}/(g\alpha\Delta T)^{\frac{1}{2}}$ for $\sigma > 1$ the diffusion of momentum out of the inner layer maintains the outer viscous layer, which has grown to thickness $O(\delta_\nu)$, where

$$\delta_\nu \sim \nu^{\frac{1}{2}}\tau^{\frac{1}{2}} \sim \frac{\nu^{\frac{1}{2}}\sigma^{\frac{1}{4}}h^{\frac{1}{4}}}{(g\alpha\Delta T)^{\frac{1}{4}}} \sim \sigma^{\frac{1}{2}}\delta_T, \tag{12}$$

the result given by Schlichting (1960). Over the scale δ_ν, however, the advection and diffusion of vorticity balance at time τ, which therefore represents the time scale for steady state of the double-layer system shown in figure 2. In this double-layer system a wall thermal layer, governed by a balance of baroclinic generation and diffusion of vorticity, is contained by an outer layer governed by a balance of advection and diffusion of vorticity.

The assumption that the boundary-layer length scales are very much less than the scale of the cavity ($\delta_\nu \ll h$) yields the criterion

$$Ra > \sigma^2. \tag{13}$$

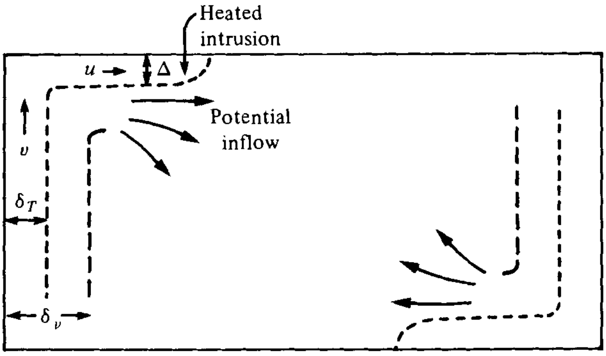

FIGURE 3. An illustration of the double-layer system discharging into the cavity. The thermal layer discharges in a layer along the horizontal boundary whereas the viscous layer enters as a potential flow.

Later in the paper it will be shown that if the criterion (13) is not satisfied a different balance is required near the heated wall (equation (25)), and a different set of scales result.

(b) *Discharge into the cavity*

The presence of the upper boundary forces both thermal and viscous vertical boundary layers to discharge into the core region of the cavity. For times greater than τ (equation (9)), the discharges are at constant flux; since the core is initially isothermal (at temperature T_0), the unheated fluid from the viscous layer discharges as a potential flow into the central part of the cavity, whereas the heated fluid from the thermal layer travels across the top of the cavity in an intrusion layer of thickness $O(\Delta)$ with velocity $u \sim Q_H/\Delta$, where $Q_H \sim v\delta_T$, the flux of fluid through the thermal boundary layer (see figure 3). The motion in the core region is driven by the boundary-layer flow and the fluid velocities there are therefore very much less than those in the intrusion layer; for the purpose of the intrusion-layer analysis the core region may be regarded as stationary. In addition to the assumption of constant flux, it is also assumed in the following that the loss of heat from an intrusion layer to the core as it travels across the cavity is small in comparison to the heat convected across. The constraints implicit in these assumptions are determined following the derivation of the relevant scales.

Under these conditions the constant flux intrusion layer is driven by a buoyancy-induced horizontal pressure gradient of $O(g\alpha\Delta T\,\Delta/ut)$, from (2), where t is the elapsed time and the layer has penetrated a distance ut along the top of the cavity. The viscous term of (1) is $O(\nu u/\Delta^2)$ and the advection term $O(u^2/ut)$; relative to the pressure gradient, these terms are of magnitudes $O(Q_H^2h^3t/\kappa\, Ra\,\Delta^5)$ and $O(Q_H^2h^3/\nu\kappa\, Ra\,\Delta^3)$ respectively. For small time the viscous effects are small and the layer is described by an inertia–buoyancy balance; an inertial layer of thickness $O(\Delta_g)$ forms, where, since $Q_H \sim \kappa\, Ra^{\frac{1}{4}}$,

$$\Delta_g \sim \frac{h}{\sigma^{\frac{1}{3}}\, Ra^{\frac{1}{6}}}. \tag{14}$$

The viscous term becomes of the same order at time $O(T_t)$, where

$$T_t \sim \frac{\kappa\, Ra\,\Delta_g^5}{Q_H^2 h^3} = \frac{h^2}{\kappa\sigma^{\frac{5}{3}}\, Ra^{\frac{1}{3}}}, \tag{15}$$

and the layer is subsequently described by a viscous–buoyancy balance, becoming of thickness $O(\Delta_\nu)$,

$$\Delta_\nu \sim \frac{\kappa^{\frac{1}{5}} h^{\frac{3}{5}} t^{\frac{1}{5}}}{Ra^{\frac{1}{10}}}. \tag{16}$$

Were the inertial layer (14) not affected by viscosity it would reach the far end wall in a time $T_g \sim l/u$, or

$$T_g \sim \frac{lh}{\kappa\sigma^{\frac{1}{3}} Ra^{\frac{5}{12}}}, \tag{17}$$

and will therefore reach the end wall without viscous influence if $T_g < T_t$, or

$$Ra > \frac{\sigma^{16}}{A^{12}}. \tag{18}$$

On the other hand the possibility exists that an inertial layer becomes viscous before the vertical boundary-layer growth is complete. This occurs if $T_t < \tau$, or

$$Ra < \sigma^{10}. \tag{19}$$

Hence if $Ra > \sigma^{10}$ an inertial intrusion layer will penetrate at least part of the way across the cavity. The condition for the layer to be distinct ($\Delta_g < h$) is $Ra > \sigma^{-2}$, which is automatically satisfied.

A viscous intrusion layer travelling the length of the cavity grows to thickness $O(\Delta_{\nu f})$ and reaches the far end wall in time $O(T_\nu)$, where

$$\Delta_{\nu f} \sim \frac{h^{\frac{3}{4}} l^{\frac{1}{4}}}{Ra^{\frac{3}{16}}} \tag{20}$$

and

$$T_\nu \sim \frac{l^{\frac{5}{4}} h^{\frac{3}{4}}}{\kappa Ra^{\frac{7}{16}}}. \tag{21}$$

In this case the intrusion layer is distinct if $\Delta_{\nu f} < h$, or

$$Ra > A^{-\frac{4}{3}}. \tag{22}$$

The assumption that Q_H is constant implies that the vertical boundary-layer growth time scale τ is less than the relevant intrusion-layer scale. For $Ra > \sigma^{10}, \tau < T_t, T_g$ and the assumption is valid for all inertial layers. For $Ra < \sigma^{10}, \tau < T_\nu$ if, from (9) and (21),

$$Ra > A^{20}. \tag{23}$$

The second assumption involved is that the loss of heat from an intrusion layer to the core by conduction is small in comparison with the flux of heat across the cavity. Since the flux across is $O(Q_H \Delta T)$ and loss in time t across the interface is $O(\kappa u t \Delta T/\Delta)$, the assumption is valid only if (since $u \sim Q_H/\Delta)\, t < \Delta^2/\kappa$. If the layer is inertial, $\Delta \sim \Delta_g$ and $t < T_t$. From (15), $T_t \sim \Delta_g^2/\nu$ and for $\sigma > 1$ the condition is satisfied. Hence the assumption is valid for all inertial layers. On the other hand, if the intrusion layer is viscous, $\Delta \sim \Delta_{\nu f}$ and the assumption is valid only if $T_\nu < \Delta_{\nu f}^2/\kappa$, or, from (20) and (21),

$$Ra > \frac{1}{A^{12}}. \tag{24}$$

If (24) is not satisfied, the scales and inequalities are no longer valid. The interpretation in this case is that, although a viscous intrusion layer may form, it quickly losses its thermal identity through vertical conduction into the core.

(c) *Core motion and the approach to steady state*

The subsequent motion in the core region is extremely complex, involving discharges from both thermal and viscous vertical boundary layers, and a detailed scaling analysis of the transient behaviour is not possible, as the scales do not separate. However, a qualitative picture of the events in the core may be constructed, and some useful scales and inequalities determined.

Consider firstly the situation for $Ra < \sigma^2$, in which case the vertical viscous boundary layer is $O(h)$. Since the diffusion of vorticity occurs over a length scale $O(h)$, the shear developed across the vertical extent of the cavity becomes significant. As a result, the negative horizontal pressure gradient in the upper half of the cavity which drives the heated fluid across (and the corresponding positive gradient in the lower half) generates a vertical pressure gradient which may influence the balance in the thermal boundary layer. A balance between the pressure forces driving the horizontal flow and the viscous forces shows that the horizontal pressure gradient is given by

$$\frac{p}{l} \sim \frac{u\nu\rho_0}{h^2}, \tag{25}$$

where u is the horizontal velocity $u \sim v\delta_T/h$. Thus the vertical gradient is $O(p/h)$, and since the viscous term is $O(\nu v/\delta_T^2)$ in the layer, the pressure term becomes important when $(p/\rho_0 h)/(\nu v/\delta_T^2) \sim 1$ or

$$\left(\frac{\delta_T}{h}\right)^3 \sim A. \tag{26}$$

From (11), equation (26) shows that, if $Ra < A^{-\frac{4}{3}}$, the viscous–buoyancy balance in the thermal layer is no longer valid, with the correct balance being between buoyancy and the pressure term, yielding the velocity scale

$$v \sim \frac{\kappa^{\frac{1}{2}} Ra\, A}{t^{\frac{1}{2}}}. \tag{27}$$

With this scale, the conduction–convection balance in the thermal layer occurs at

$$\tau \sim \frac{l^2}{\kappa Ra^2}, \tag{28}$$

by which time the layer has reached thickness

$$\delta_T \sim \frac{l}{Ra}. \tag{29}$$

Thus if $Ra < A^{-\frac{4}{3}}$, the vertical thermal layer continues to advance unidirectionally (since $\partial T/\partial y = 0$ on the upper and lower boundaries) until the thickness (29) is reached; for $Ra < 1$, the layer encompasses the entire cavity before convection becomes important. On the other hand, if $Ra > A^{-\frac{4}{3}}$, (11) shows that $\delta_T < l$ and the thermal layer is distinct.

However, this distinct vertical thermal layer resulting in either case for $Ra > 1$ may be destroyed in a number of ways. First, if $1 < Ra < A^{-\frac{4}{3}}$, the heated horizontal intrusion layers discharged from the distinct vertical thermal layer are of thickness $O(h)$, and any vertical temperature structure is annihilated. This input of heat to the core over the height of the cavity erodes the steep temperature gradient at the edge of the thermal layer, which effectively advances across the cavity. Secondly, if $A^{-\frac{4}{3}} < Ra < \sigma^2$, the diffusion of vorticity is again over a length scale h, spreading the horizontal intrusion layer to $O(h)$ with the same result as in the previous case. Thirdly, if $Ra < A^{-12}$, potentially distinct heat intrusion layers move into the core but quickly lose their heat content by vertical conduction, again effectively thickening the vertical thermal layer.

As the Rayleigh number increases beyond $A^{-\frac{4}{3}}$, A^{-12}, and σ^2, distinct vertical boundary layers form, ejecting heated fluid in distinct horizontal layers which convect heat across the cavity without significant loss by conduction to the core. As subsequent layers traverse the core, a stable vertical temperature gradient is set up. The core fills with heated fluid by horizontal layering, filling occurring in the time taken for all of the fluid to pass through the thermal boundary layer,

$$T_f \sim \frac{hl}{\kappa Ra^{\frac{1}{4}}}. \tag{30}$$

The nature of the layering changes with increasing Ra, with viscous layers occurring for $Ra < \sigma^{10}$, inertial layers becoming viscous for $\sigma^{10} < Ra < \sigma^{16}A^{-12}$, and purely inertial layers for $Ra > \sigma^{16}A^{-12}$.

Thus for a given set of non-dimensional parameters, the flow may be broadly classified into one of three regimes. The first regime, $Ra < 1$, is predominantly conductive, with vertical isotherms moving out from the boundaries as the thermal layer advances across the cavity, approaching a linear horizontal temperature gradient at steady state. Although the horizontal gradient drives a weak circulation, convection is negligible in comparison to horizontal conduction of heat and the fluid motion plays no part in the heat transfer process. Steady state is achieved in the conduction time scale $T_c \sim l^2/\kappa$.

The second flow regime occurs for Rayleigh numbers greater than $A^{-\frac{4}{3}}$, A^{-12}, and σ^2, or, since $A^{-\frac{4}{3}} \leqslant A^{-12}$ for $A \leqslant 1$, for $Ra > Ra_c$, where the critical Rayleigh number Ra_c is defined by

$$Ra_c \sim \max(\sigma^2, A^{-12}). \tag{31}$$

In this case, horizontal intrusion layers convect heat across the cavity, reinforcing the conducting thermal layers on the end walls and generating predominantly horizontal isotherms in the core. The core fills by horizontal layering, with a first estimate of the steady-state time being given by T_f.

The third region, $1 < Ra < Ra_c$, is one of transition between these conductive and convective extremes, with convective effects becoming evident as Ra approaches Ra_c. The steady-state time will lie between T_c and T_f.

One further mechanism may be of importance in the convective regime. Since the heated intrusion layers discharged from the vertical thermal layer are of thickness small in comparison with h, the thermal layer is entraining over a length greater than the thickness of the discharge. By symmetry, the horizontal intrusion layer incoming to the vertical thermal layer is of the same thickness as the discharging layer. Thus

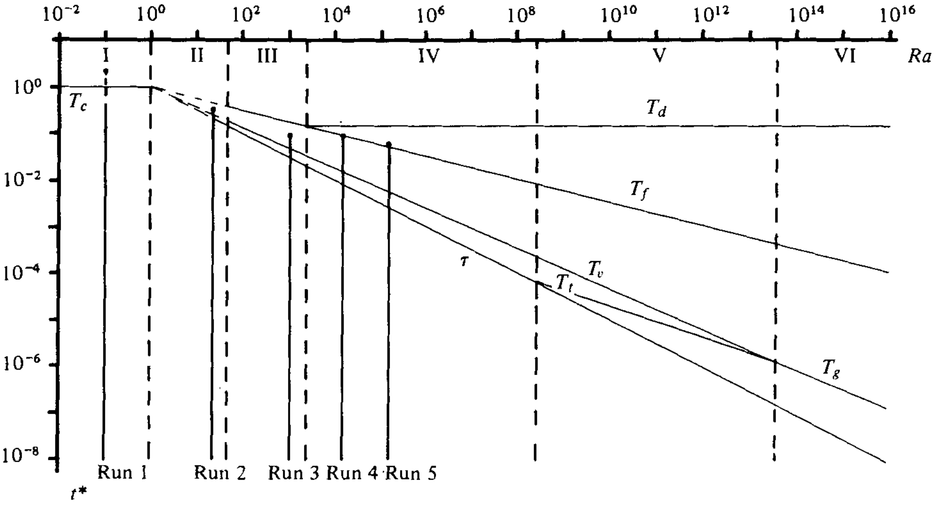

FIGURE 4. The variation with Ra of the various time scales in their regions of validity for the case $\sigma = 7, A = 1$. The boundaries between flow regimes I–VI are indicated by the broken vertical lines and computation runs 1–5 by the solid vertical lines, terminating at the time at which steady state was numerically achieved.

the entrainment length acts as a distributed sink to the incoming intrusion layer, which spreads against buoyancy to meet the sink. Since these horizontal layers have not lost heat to the core, the effect of this spreading is a tilting of the isotherms beyond the horizontal and the consequent generation of internal waves of frequency $O(\omega)$,

$$\omega \sim \frac{N}{(1+A^2)^{\frac{1}{2}}}, \tag{32}$$

where the Brunt–Väisälä frequency is defined by $N \sim (\nu\kappa\, Ra)^{\frac{1}{2}}/h^2$.

This internal wave motion is damped by a combination of viscosity and the draining of momentum into the vertical boundary layers; an upper estimate for the decay time is given by $T_d \sim h^2/\nu$. Since steady state cannot be achieved before all wave motion has decayed or before the filling time T_f, the convective regime steady-state time is given by the maximum of T_d and T_f. For $Ra > \sigma^4 A^{-4}$, $T_f < T_d$, and the decaying wave motion may extend steady state beyond T_f. In this case, the total heat transfer across the cavity rises to a peak as the core isotherms tilt beyond the horizontal and subsequently approaches a steady value in a decaying oscillation as the internal wave motion dies away. On the other hand, if $Ra < \sigma^4 A^{-4}$, $T_d < T_f$, and all wave motion has decayed before the cavity is filled. In this case, the approach to steady state is regular as the cavity fills, implying that all internal wave motion is quickly damped and will not be evident.

(*d*) *Overall evolution to steady state*

The results of the previous sections may be summarized to provide an overall picture of the evolution of the flow from initiation to steady state for a particular set of parameter values. The flow may be classified as convective, conductive, or transitional, depending on the relative values of Ra, 1, and Ra_c. Within the convective

Regime		Time scale (t^*)	Parameter	Equation	Comments
I	$Ra < 1$	A^{-2}	T_c		Steady state by the thermal boundary layer encompassing the entire cavity. Heat transfer by conduction
II	$1 < Ra < \sigma^2$	$A^{-2} \rightarrow A^{-1} Ra^{-\frac{1}{4}}$	$T_c \rightarrow T_f$	(30)	Steady state by a combination of the thermal boundary advancing across the cavity and convective effects being dissipated by vertical diffusion. Both convection and conduction participate in the heat transfer
III	$\sigma^2 < Ra < \sigma^4 A^{-4}$	$Ra^{-\frac{1}{2}}$	τ	(9)	Thermal and viscous boundary layers steady and distinct
		$A^{-\frac{5}{4}} Ra^{-\frac{7}{16}}$	T_ν	(20)	Horizontal viscous intrusion layer reaches far wall
		$A^{-1} Ra^{-\frac{1}{4}}$	T_f	(30)	Steady state by horizontal layering. No internal wave motion, convection becoming important in the heat transfer
IV	$\sigma^4 A^{-4} < Ra < \sigma^{10}$	$Ra^{-\frac{1}{2}}$	τ	(9)	Thermal and viscous boundary layers steady and distinct
		$A^{-\frac{5}{4}} Ra^{-\frac{7}{16}}$	T_ν	(20)	Horizontal viscous intrusion layer reaches far wall. Internal wave motion begins
		$A^{-1} Ra^{-\frac{1}{4}}$	T_f	(30)	Cavity fitted by horizontal layering. Internal wave motion present
		σ^{-1}	T_d		Steady state by decay of internal wave motion. Convection-dominated heat transfer
V	$\sigma^{10} < Ra < \sigma^{16} A^{-12}$	$Ra^{-\frac{1}{2}}$	τ	(9)	Thermal and viscous boundary layers steady and distinct
		$\sigma^{-\frac{5}{3}} Ra^{-\frac{1}{3}}$	T_i	(15)	Horizontal inertial intrusion layer becomes viscous
		$A^{-\frac{5}{4}} Ra^{-\frac{7}{16}}$	T_ν	(20)	Viscous intrusion layer reaches far wall. Internal wave motion begins
		$A^{-1} Ra^{-\frac{1}{4}}$	T_f	(30)	Cavity filled by horizontal layering. Internal wave motion present
		σ^{-1}	T_d		Steady state by decay of internal wave motion. Convection-dominated heat transfer
VI	$\sigma^{16} A^{-12} < Ra$	$Ra^{-\frac{1}{2}}$	τ	(9)	Thermal and viscous boundary layers steady and distinct
		$A^{-1} \sigma^{-\frac{1}{3}} Ra^{-\frac{5}{12}}$	T_g	(17)	Horizontal inertial intrusion layer reaches far wall. Internal wave motion begins
		$A^{-1} Ra^{-\frac{1}{4}}$	T_f	(30)	Cavity filled by horizontal layering. Internal wave motion present
		σ^{-1}	T_d		Steady state by decay of internal wave motion. Convection-dominated heat transfer

TABLE 1

regime, the parameter σ^2A^{-4} determines the nature of the approach to steady state. Further, the parameters $A^{-\frac{4}{3}}$, σ^{10}, and $\sigma^{16}A^{-12}$ define a number of sub-regimes of the broader classifications. For the values $\sigma > 1$, $A \leqslant 1$ considered here, six possible orderings of these critical *Ra* values are possible, depending on the relative values of σ and A, each ordering yielding a different set of transient flow regimes. An examination of all these possibilities is beyond the scope of this paper, and only the case which arises for $\sigma > A^{-6}$, which yields the ordering

$$1 \leqslant A^{-\frac{4}{3}} < A^{-12} < \sigma^2 < \sigma^4A^{-4} < \sigma^{10} < \sigma^{16}A^{-12}$$

is discussed below. This case is the only one for which $Ra_c = \sigma^2$, and, since the parameters $A^{-\frac{4}{3}}$ and A^{-12} are not relevant, no generality is lost by taking the special case $A = 1$. The remaining possible orderings can only arise if $A < 1, \sigma < A^{-6}$, and will be treated in a subsequent paper.

The evolution to steady state in each of the six regimes defined by the parameter values is summarized by figure 4, which shows for $A = 1$ and $\sigma = 7$ the variation with *Ra* of the relevant time scales (non-dimensionalized by $h^2\kappa^{-1}$) for their regimes of validity, and by table 1, which briefly describes the hierarchy of time scales which divide each regime into a number of transient sub-regimes.

3. Numerical procedures

In order to test the validity of the scale analysis and interpretation of the previous sections, a number of numerical solutions have been obtained for the case $A = 1$ and parameter values such that the principal flow regimes are traversed. The finite-difference method used for the numerical solution of the set (1)–(6) is based on the scheme proposed by Chorin (1968), which uses the raw vaiiables of velocity and pressure rather than the derived stream-function–vorticity formulation.

A number of modifications to the original scheme were found to be desirable, the most important of which involved alternations to the methods of obtaining the auxiliary velocity field and the iterative solution for new time-step pressures and velocities. Briefly, Chorin's scheme involves the solution (explicit or implicit) of the momentum equations, with the pressure term deleted, for an auxiliary velocity field, which, in conjunction with the full momentum and continuity equations, is used to construct an iterative algorithm for the new time-step velocities and mid time-step pressures. The first modification incorporated an outer iteration loop, where the last known pressure is used in the generation of the auxiliary field, which is now an estimate for the velocities, followed by the solution for the pressure increment and a new velocity increment which are inserted back into the momentum equations, the process continuing until conveigence is achieved. Only a small number of outer iterations is generally required, depending of course on the convergence criterion, and the method proved more accurate and not significantly slower than the original.

The second modification was concerned with the (now) inner iteration; the solution for the new pressure increments. In the original scheme, the algorithm constructed was essentially the iterative solution of a Poisson equation for pressure, defined on two intertwined meshes coupled on the boundary by continuity. At high Rayleigh numbers, oscillations between the meshes were inclined to develop unless higher-order differencing on the boundary was used. It proved simpler to redefine the entire problem on a staggered (MAC) mesh, with pressures defined in the centres of the mesh rectangles and velocities on the sides in the usual way. In this way, the Poisson equation is defined on a single mesh, with the pressure boundary conditions being directly obtained from the momentum equations in a manner consistent with continuity.

Before differencing, the set (1)–(6) was non-dimensionalized according to the scheme

$$\left.\begin{aligned} &X = x/h, \quad Y = y/h, \quad t^* = t\kappa/h^2, \\ &U = uh/\nu, \quad V = vh/\nu, \quad T^* = (T-T_0)/\Delta T, \\ &P = ph^2/\rho_0\nu^2, \end{aligned}\right\} \tag{33}$$

and the transport equations written in conservative form. A check on the progress of the integration is made by the evaluation of a measure of the heat transfer, the Nusselt number, at the heated end and at the centre-line of the cavity. The Nusselt number Nu is defined as

$$Nu = \frac{1}{2A}\int_0^1 \left(\sigma UT^* - \frac{\partial T^*}{\partial X}\right)_X dy, \tag{34}$$

where at the heated end $X = 0$, and at the centre-line $X = \frac{1}{2}A^{-1}$. When these two values of Nu, which measure the total heat transfer in the horizontal direction at each station, have reached steady values and are equal, within a prescribed error, steady state is assumed to have been reached. This is confirmed by the iteration count; at steady state each time step is completed in a minimum number of inner and outer iterations, the actual number depending on the convergence criteria in each case.

A check on the conservation properties of the algorithm is also made periodically. Because of the symmetry of the problem, which is not explicitly built into the algorithm, the Nusselt numbers at each end must be equal at any instant; the total non-dimensional heat content of the cavity is always zero. Hence conservation of energy is checked by a periodic integration of the temperature field over the entire cavity, which should be zero within a prescribed error.

The remaining points of interest in the numerical context are those of stability and accuracy. These questions are complex for this type of problem and a vast literature exists (see Roache 1972); in the present context it is sufficient to note that, for accurate spatial and temporal representation of the solution (and hence stability as well), limits on time-step and mesh size are enforced by the time and length scales of the problem, in addition to any other stability criterion in use. For example, for convection-dominated flows, it is essential that at least two mesh points are contained in the boundary layer at each vertical level. Hence for a uniform grid of n_x points in the X direction, with spacing h_x,

$$h_x < \tfrac{1}{2}\delta_\nu, \quad \text{or} \quad An_x > 2\,Ra^{\frac{1}{4}}\sigma^{-\frac{1}{2}}. \tag{35}$$

For Prandtl number $\sigma \sim O(1)$, (35) yields, for $Ra = 10^6$ for example, $An_x > 63$. Hence, with $A \leqslant 1$, maintaining a reasonable mesh aspect ratio may mean an excessive number of mesh points and consequent storage problems, together with an increase in computation time. Similarly, the time-step size is limited by the time scale of the internal wave motions, obtained from (32).

The use of such devices as non-uniform grids and specialist differencing methods were introduced and alleviated the problem somewhat; however these schemes frequently introduced additional complications and a significant extension of the range of Rayleigh numbers amenable to numerical solution by finite-difference methods is unlikely.

In view of this, solutions in the present study have been obtained for a limited range of Rayleigh and Prandtl numbers only. Even within this range, the larger-Rayleigh-number problems proved costly in terms of storage and computation time and the additional expense of attempting to extend the range was not warranted.

4. Results and discussion

The computations were directed at traversing the six transient flow regimes defined for the case $A = 1, \sigma > A^{-6}$. All computations were carried out on square, uniformly spaced grids, the time step and grid spacing being determined initially from (32) and (35). These were occasionally changed as the result of numerical experiment.

The first series of computations was for $\sigma = 7$ and Ra taking the values 10^{-1}, $2{\cdot}1 \times 10^{1}$, 10^{3}, $1{\cdot}4 \times 10^{4}$ and $1{\cdot}4 \times 10^{5}$, traversing regimes I to IV. The results of these computations are shown in figures 5–9; in each figure the variation with t^* of the Nusselt numbers at the hot end (Nu_E) and centre line (Nu_c) of the cavity is shown, indicating the progression of the flow to steady state. The temperature and flow fields at steady state are also shown in each case and, in some cases, the fields at some transient stage are also given, together with the progression of the lower half of the $T^* = 0$ isotherm with t^*. In addition, each run in this series is depicted as a vertical line on figure 4, terminating at the time at which the computation was halted. The results of these computations are discussed below.

Run 1: $\sigma = 7$, $Ra = 10^{-1}$. In this case a completely conduction-dominated flow (regime I) is indicated. The Nusselt numbers at the end and centre line of the cavity (figure 5*a*) monotonically approach the pure conduction value unity from above and below as the thermal boundary layer progresses across the cavity and the temperature gradients and the end and centre decrease and increase to a linear gradient across the cavity (figure 5*c*). This gradient drives an extremely weak circulation (figure 5*b*) with no effect on the heat transfer. The approach to steady state consists merely of vertical isotherms moving out from the end walls gradually approaching the steady result. Because of the extremely slow convergence to steady state, the computation was halted at $t^* = 0{\cdot}4$ and restarted with a linear horizontal temperature gradient; the algorithm quickly converged to the flow field shown in figure 5(*b*) without a noticeable alteration to the temperature structure.

Run 2: $\sigma = 7$, $Ra = 2{\cdot}1 \times 10^{1}$. Again a conduction-dominated flow with some convective effects is expected. The Nusselt numbers (figure 6*a*) and the steady-state flow and temperature fields (figure 6*b*, *c*) display the same characteristics as the previous case, although the velocities are higher and a very slight convective tilt is present in the isotherms. Steady state is indicated numerically at $t^* = 0{\cdot}31$, compared with the time predicted by (30), $T_f^* \sim 0{\cdot}47$ (figure 4).

Run 3: $\sigma = 7$, $Ra = 10^{3}$. In this case Ra has passed into regime III and convective effects are expected to be present. However, since $Ra < \sigma^4 A^{-4}$, internal wave motion will be damped before the cavity filling time and the approach to steady state will

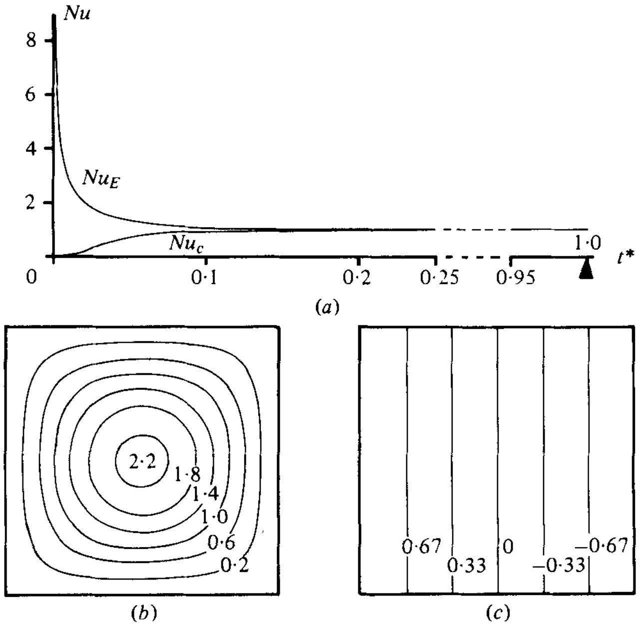

FIGURE 5. The numerical results for run 1, $\sigma = 7$, $Ra = 10^{-1}$. (*a*) The dependence of Nu_c and Nu_E on t^*; (*b*) the steady-state streamlines; and (*c*) the steady-state isotherms. The solid triangle on (*a*) indicates the time at which the streamlines and isotherms are taken. The numerical values on (*b*) and (*c*) are values of $(\psi/\nu) \times 10^5$ and T^* respectively.

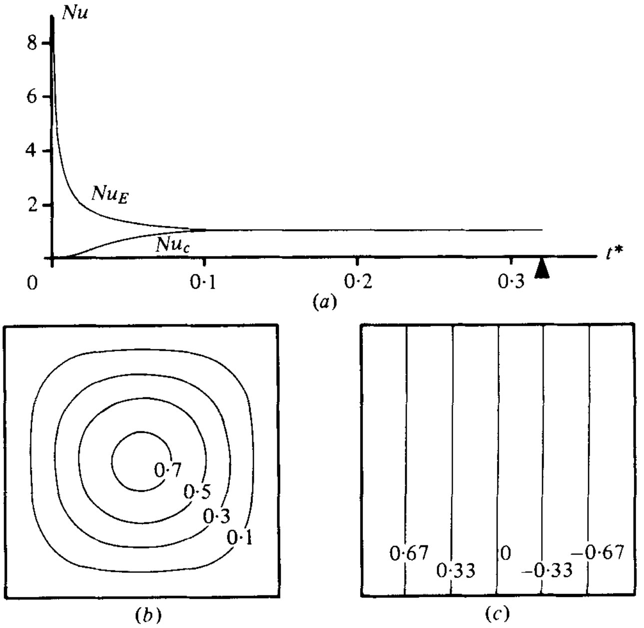

FIGURE 6. The numerical results for run 2, $\sigma = 7$, $Ra = 21$. (*a*) The dependence of Nu_c and Nu_E on t^*; (*b*) the steady-state streamlines; and (*c*) the steady-state isotherms. The solid triangle on (*a*) indicates the time at which the streamlines and isotherms are taken. The numerical values on (*b*) and (*c*) are values of $(\psi/\nu) \times 10^2$ and T^* respectively.

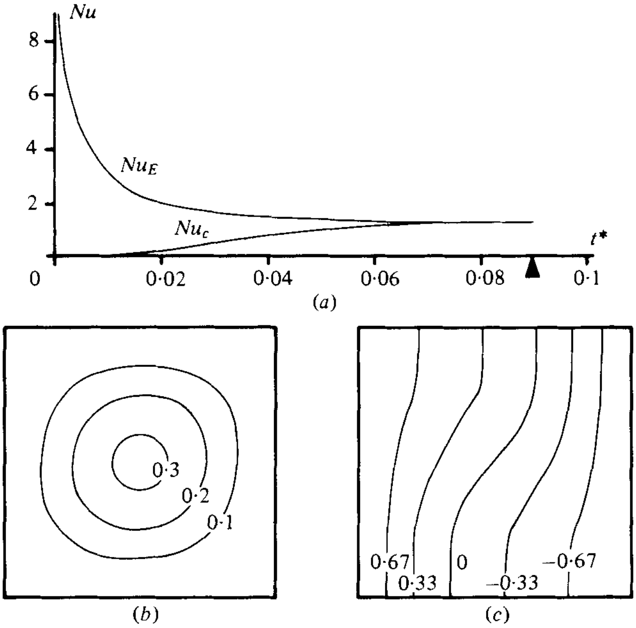

FIGURE 7. The numerical results for run 3, $\sigma = 7$, $Ra = 10^3$. (a) The dependence of Nu_c and Nu_E on t^*; (b) the steady-state streamlines; and (c) the steady-state isotherms. The solid triangle on (a) indicates the time at which the streamlines and isotherms are taken. The numerical values on (b) and (c) are values of ψ/ν and T^* respectively.

be monotonic. This is confirmed by figure 7 (a), showing the Nusselt numbers approaching the steady value 1·25 from above and below, the increased steady-state value indicating the increased importance of convection. At steady state, achieved numerically at $t^* = 0{\cdot}09$, compared with $T_f^* \sim 0{\cdot}18$, the flow and temperature fields (figure 7b, c) show a stronger circulation, some convective tilt to the isotherms in the core region, and the presence of a conduction region near the end walls. At all times previous to steady state the temperature field shows only a gradually increasing convective effect and again no transient result is shown.

Run 4: $\sigma = 7$, $Ra = 1{\cdot}4 \times 10^4$. The convective regime IV is relevant in this case and, in addition to increasing convection, evidence of internal wave motion is expected. Figure 8 (a) shows Nu_c rising to a peak at $t^* = 0{\cdot}026$ and subsequently dropping away to the steady value 3·31 at $t^* = 0{\cdot}08$, indicating the passage of one wave heavily damped. At $t^* = 0{\cdot}014$, before the peak in heat transfer, the flow and temperature fields (figure 8b, c) show a rapid increase in velocities, the presence of a boundary layer, the divergence of the intrusion layers as they enter the core (indicated by the tilt in the streamline pattern), and the convective effect on the temperature field. At steady state (figure 8d, e), the internal wave activity has decayed, the velocities decreased from their maximum values, and the streamlines are nearly parallel in the core. The isotherms are approximately horizontal in the core, indicating the dominance of convection, turning sharply into well-defined boundary regions conducting heat in and out of the cavity. The $T^* = 0$ isotherm (figure 8f) becomes tilted beyond the horizontal near the peak in heat transfer and slowly decays to its steady configuration as the wave motion decays.

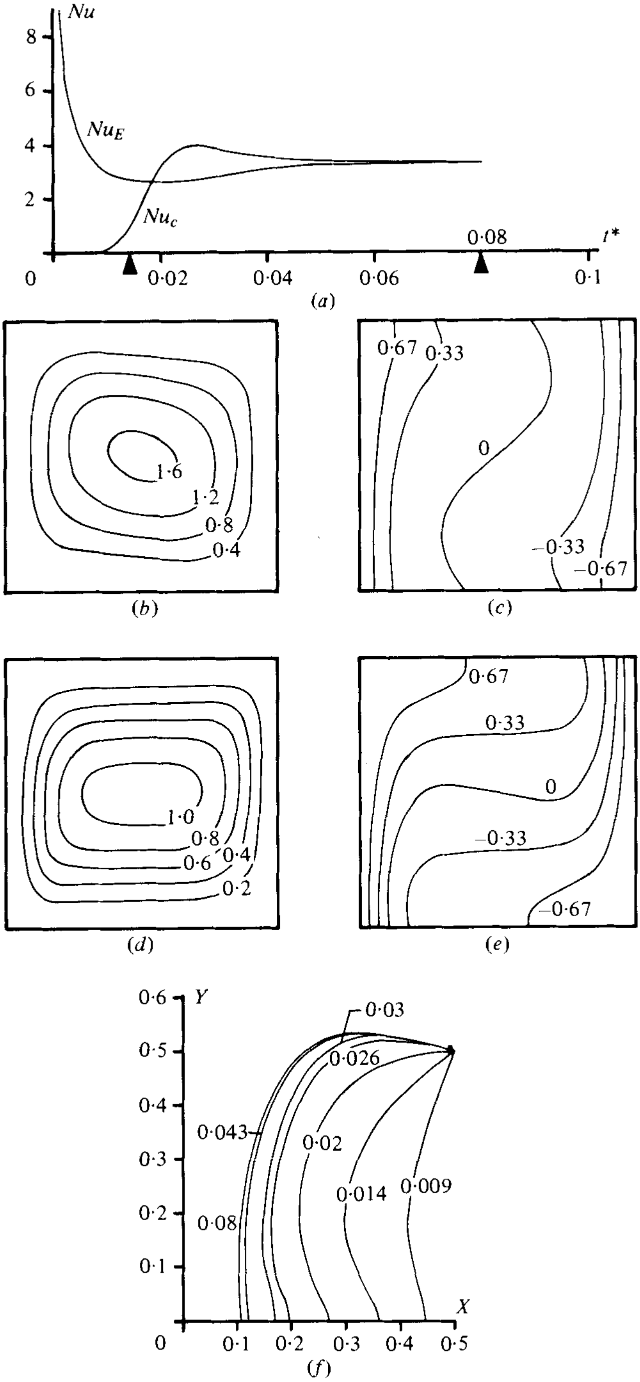

FIGURE 8. The numerical results for run 4, $\sigma = 7$, $Ra = 1{\cdot}4 \times 10^4$. (*a*) The dependence of Nu_c and Nu_E on t^*; (*b*, *c*) the streamlines and isotherms at $t^* = 0{\cdot}014$; (*d*, *e*) the streamlines and isotherms at steady state; and (*f*) the variation of the lower half of the $T^* = 10$ isotherm with t^*. The solid triangles on (*a*) indicate the times at which the transient and steady-state results are taken. The numerical values on the streamline and isotherm plots are values of ψ/ν and T^* respectively.

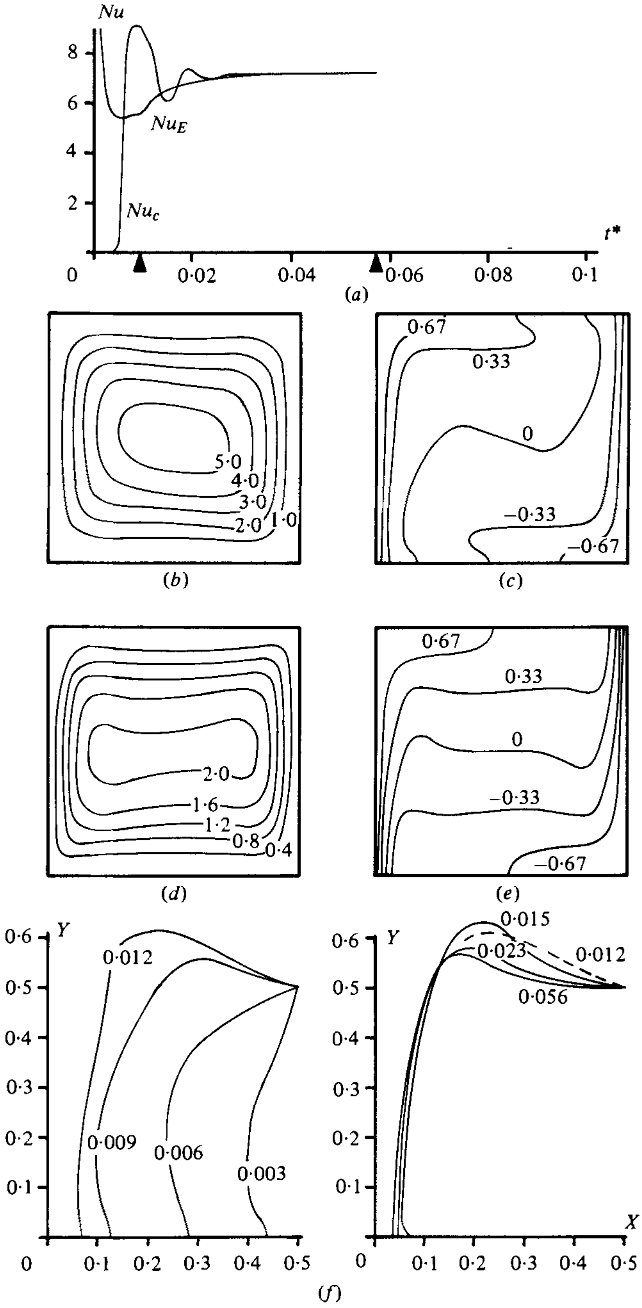

FIGURE 9. The numerical results for run 5, $\sigma = 7$, $Ra = 1{\cdot}4 \times 10^5$. (*a*) The dependence of Nu_c and Nu_E on t^*; (*b*, *c*) the streamlines and isotherms at $t^* = 0{\cdot}009$; (*d*, *e*) the streamlines and isotherms at steady state; and (*f*) the variation of the lower half of the $T^* = 0$ isotherms with t^*. The solid triangles on (*a*) indicate the times at which the transient and steady-state results are taken. The numerical values on the streamline and isotherm plots are values of ψ/ν and T^* respectively.

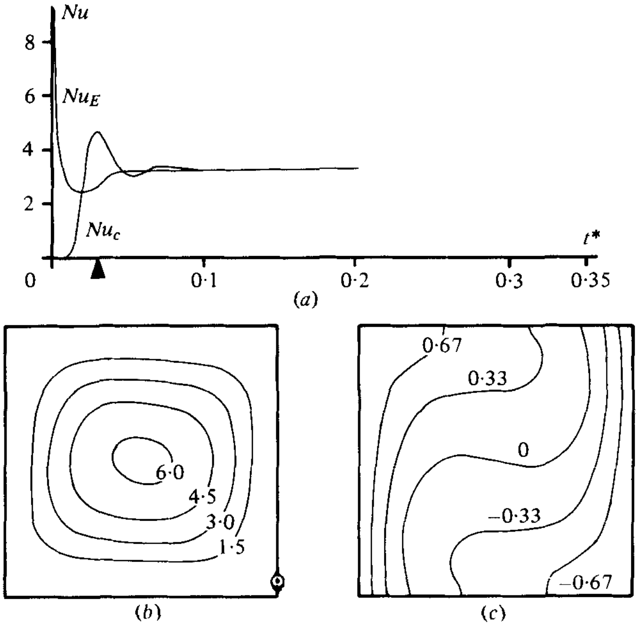

FIGURE 10. The numerical results for run 6, $\sigma = 2$, $Ra = 1{\cdot}4 \times 10^4$. (*a*) The dependence of Nu_c and Nu_E on t^*; and (*b*, *c*) the streamlines and isotherms at $t^* = 0{\cdot}30$, before steady state. The solid triangle on (*a*) indicates the time at which the transient results are taken. The numerical values on (*b*) and (*c*) are values of ψ/ν and T^* respectively.

Run 5: $\sigma = 7$, $Ra = 1{\cdot}4 \times 10^5$. In this case the flow description remains in regime IV, although convective effects and the internal wave activity are expected to be stronger than in the previous case. The centre-line Nusselt number (figure 9*a*) shows evidence of strong internal wave motion surviving for several periods of $O(0{\cdot}01)$, compared with the value $2\pi/\omega^*$, from (32), of $O(0{\cdot}009)$, decaying away to a steady-state $Nu = 7{\cdot}24$ at $t^* = 0{\cdot}056$, between $T_f^* \sim 0{\cdot}052$ and $T_d^* \sim 0{\cdot}143$. The transient flow and temperature fields (figure 9*b*, *c*) taken at $t^* = 0{\cdot}009$, near the first peak in heat transfer and hence at near-peak core velocities, show a similar tilt to the streamline pattern as in the previous case, well-defined boundary regions, and a strongly tilted $T^* = 0$ isotherm in the core. The tilted streamlines are evidence of the viscous boundary layer entering the core, while the $T^* = 0{\cdot}33$ and $T^* = -0{\cdot}33$ isotherms clearly show a heated intrusion layer entering the core. In this case the intrusion layer is viscous and, at $t^* = 0{\cdot}009$, has thickness $O(0{\cdot}12)$, of the same order that is shown on figure 9(*c*), $O(0{\cdot}14)$. At steady state (figure 9*d*, *e*) the flow has passed through several oscillations and has slowed considerably, with strong boundary layers present on the end walls. The isotherms in the core region are essentially horizontal, turning sharply into conducting boundary layers. Figure 9(*f*) shows the $T^* = 0$ isotherm developing a strong tilt beyond the horizontal in the core region, and subsequently decaying away to a horizontal configuration at steady state, with a horizontal gradient at the edge of the boundary layer driving the flow across the cavity.

To access regimes V and VI with $\sigma = 7$ requires Rayleigh numbers of the order of 10^9 and 10^{13} respectively. To avoid the numerical difficulties associated with parameter

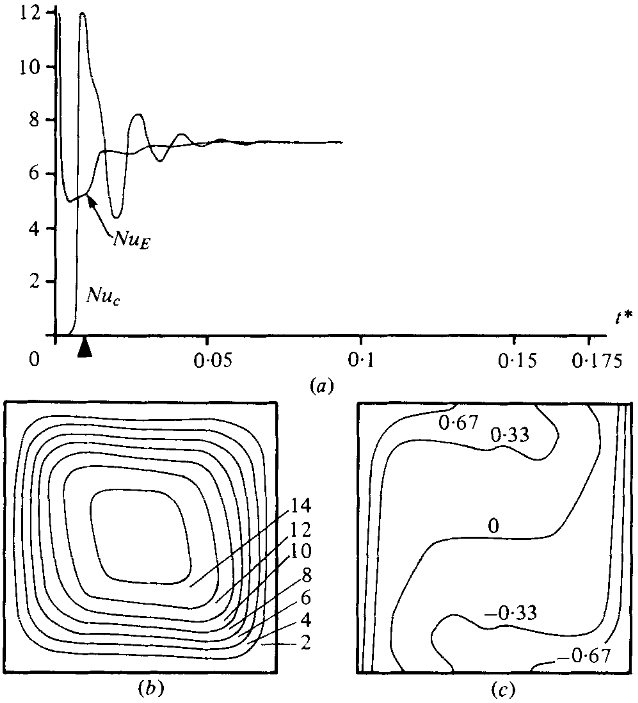

FIGURE 11. The numerical results for run 7, $\sigma = 2$, $Ra = 1{\cdot}4 \times 10^5$. (a) The dependence of Nu_c and Nu_E on t^*; and (b, c) the streamlines and isotherms at $t^* = 0{\cdot}01$, before steady state. The solid triangle on (a) indicates the time at which the transient results are taken. The numerical values on (b) and (c) are values ψ/ν and T^* respectively.

values of this magnitude, flows in these regimes were generated by a reduction in Prandtl number. Hence a second series of computations were undertaken with $\sigma = 2$, and Ra taking the values $1{\cdot}4 \times 10^4$ and $1{\cdot}4 \times 10^5$, accessing regimes V and VI respectively. The results of these runs are shown in figures 10 and 11.

Run 6: $\sigma = 2$, $Ra = 1{\cdot}4 \times 10^4$. Although this computation lies in regime V, the reduction in both σ and Ra precludes direct comparison with run 5 in regime IV. In particular, both the period of the internal waves and the filling-time estimate T_f increase over run 5, as does the decay time T_d. Figure 10(a) shows the Nusselt number variation with t^*, indicating the presence of internal waves of period $O(0{\cdot}042)$, in comparison to a period $O(0{\cdot}053)$ suggested by (32). The transient streamlines and isotherms taken at $t^* = 0{\cdot}03$, near the first peak in heat transfer, again show the features typical of the convective regime; a tilted streamline pattern and $T^* = 0$ isotherm in the core, evidence of an entering layer of heated fluid, and a conducting boundary region. At steady state, achieved numerically at $t^* = 0{\cdot}2$, the Nusselt number has approached 3·31, identical to the result for run 4 (with the same Ra value), and the steady-state flow and temperature fields are also indistinguishable from those of run 4 and are not shown. A discussion of the dependence of both the steady and transient behaviour on Prandtl number is given below.

Run 7: $\sigma = 2$, $Ra = 1{\cdot}4 \times 10^5$. In this case the purely inertial regime VI is relevant. The centre-line Nusselt number (figure 11a) indicate the presence of strong internal waves of period $O(0{\cdot}019)$, surviving for many periods before decay to the steady $Nu = 7{\cdot}24$, the same as the result for run 5. The period predicted from (32) for this computation is 0·017, in good agreement with the observed value. At $t^* = 0{\cdot}01$, near the first peak, the convective effects are again clearly present (figure 11*b*, *c*). In this case the $T^* = 0{\cdot}33$ and $T^* = -0{\cdot}33$ isotherms show an entering layer of heated fluid which has begun to diverge to meet the distributed sink on the cold and hot walls respectively. At steady state, the flow and temperature fields are indistinguishable from those of run 5 with the same Ra value and are again not shown.

The results of runs 6 and 7 also raise the question of the dependence of the flow and heat transfer properties on the value of the Prandtl number. It has already been indicated that the steady results from these computations were identical to those of runs 4 and 5 respectively, which have corresponding Ra values, demonstrating that indeed the steady result is independent of σ. This is to be expected since, in terms of heat transfer, as $Ra \to \infty$ for fixed A, the steady Nusselt number is given by the temperature gradient across the thermal boundary layer,

$$\begin{aligned} Nu &\sim \frac{L}{2\Delta T}\frac{\Delta T}{\delta_T} \\ &\sim \frac{Ra^{\frac{1}{4}}}{2A}, \end{aligned}$$

independent of σ. On the other hand small values of Ra lead to a conduction-dominated process, with $Nu \sim O(1)$, again independent of σ.

A comparison of figure 8(*a*) with 10(*a*) and figure 9(*a*) with 11(*a*) however clearly shows that the approach to steady state is markedly different. In both cases, the reduction in σ leads to stronger internal wave action surviving for more periods. Again this is to be expected, since although the steady-state result may be σ independent, the divisions in transient flow regimes which determine the mechanism by which steady state is achieved are dependent on σ.

5. Conclusions

The completed results indicate that, for fixed A and σ and increasing Ra, the description of the flow changes from conduction dominated to convection dominated as Ra increases beyond the values of unity and Ra_c. The conduction-dominated flows $Ra < 1$ are in the sense of Batchelor (1954) (small horizontal temperature gradients), and exhibit the slow spin-up illustrated in figures 5 and 6, extending into the transition regime $1 < Ra < Ra_c$, where, for the case treated in detail numerically, $A = 1$, $\sigma > 1$, $Ra_c \sim \sigma^2$. On the other hand, flows in the sense of Gill (1966) arise for $Ra > Ra_c$, with the approach to steady state being either regular through horizontal layering in the core or oscillatory through the decay of internal wave motion, depending on the relative values of Ra and $\sigma^4 A^{-4}$, illustrated in figures 7–11. The conductive flows described by Cormack, Leal & Imberger (1974) can only be achieved for $A < 1$, $1 < \sigma < A^{-6}$, and their transient properties will be discussed in a subsequent paper.

Although the steady state of these flows is independent of the value of the Prandtl number, it is evident that the transient flows may depend strongly on σ. Thus different transient flows may belong to different regimes, but ultimately converge to identical steady states.

Finally, the potentially oscillatory nature of the convective flows is of considerable importance to environmental flows. In particular, at times of minimum heat transfer, the streamline patterns indicate a tendency towards the formation of closed cells at either end of the cavity. Should the forcing time scale be such that the flow does not progress beyond this time or even reinforces the effect, undesirable heat or mass may be dispersed inefficiently, or even returned to its injection point.

This work was supported in part by the Australian Research Grants Committee under contract number B71/17641 and jointly by the Public Works Department and the Metropolitan Water Supply, Sewerage and Drainage Board, Western Australia, under grant number RG0-61-2100-77.

REFERENCES

BATCHELOR, G. K. 1954 *Quart. J. Appl. Math.* **12**, 209.

BRAUN, W. H., OSTRACH, S. & HEIGHWAY, J. E. 1961 *Int. J. Heat Mass Transfer* **2**, 121.

CHORIN, A. J. 1968 *Maths. Comp.* **22**, 745.

CORMACK, D. E., LEAL, L. G. & IMBERGER, J. 1974 *J. Fluid Mech.* **65**, 209.

CORMACK, D. E., LEAL, L. G. & SEINFELD, J. H. 1974 *J. Fluid Mech.* **65**, 231.

COTTON, I., AYYASWAMY, P. S. & CLEVER, R. M. 1974 *Int. J. Heat Mass Transfer* **17**, 173.

DE VAHL DAVIS, G. 1968 *Int. J. Heat Mass Transfer* **11**, 1675.

ECKERT, E. R. G. & CARLSON, W. O. 1961 *Int. J. Heat Mass Transfer* **2**, 106.

ELDER, J. W. 1965 *J. Fluid Mech.* **23**, 77.

GILL, A. E. 1966 *J. Fluid Mech.* **26**, 515.

IMBERGER, J. 1974 *J. Fluid Mech.* **65**, 247.

NEWELL, M. E. & SCHMIDT, F. W. 1970 *J. Heat Transfer* **92**, 159.

QUON, C. 1972 *Phys. Fluids* **15**, 12.

ROACHE, P. J. 1972 *Computational Fluid Dynamics*. Albuquerque: Hermosa.

SCHLICHTING, H. 1960 *Boundary Layer Theory*, 4th edn. McGraw-Hill.

SZEKELY, J. & TODD, M. R. 1971 *Int. J. Heat Mass Transfer* **14**, 467.

WILKES, J. O. & CHURCHILL, S. W. 1966 *A.I.Ch.E. J.* **12**, 161.